Proceedings of FEDSM'00
2000 ASME Fluids Engineering Division Summer Meeting
June 11-15, 2000, Boston, MA

FEDSM00-XXXX

SPARGER EFFECTS ON GAS VOLUME FRACTION DISTRIBUTIONS IN VERTICAL BUBBLE-COLUMN FLOWS AS MEASURED BY GAMMA-DENSITOMETRY TOMOGRAPHY

D. L. George, K. A. Shollenberger, and J. R. Torczynski
Engineering Sciences Center
Sandia National Laboratories[1]
Albuquerque, New Mexico 87185-0834 USA

ABSTRACT

Gamma-densitometry tomography is applied to study the effects of sparger hole geometry, gas flow rate, column pressure, and phase properties on gas volume fraction profiles in bubble columns. Tests are conducted in a column 0.48 m in diameter, using air and mineral oil, superficial gas velocities ranging from 5 to 30 cm s^{-1}, and absolute column pressures from 103 to 517 kPa. Reconstructed gas volume fraction profiles from two sparger geometries are presented. The development length of the gas volume fraction profile is found to increase with gas flow rate and column pressure. Increases in gas flow rate increase the local gas volume fraction preferentially on the column axis, whereas increases in column pressure produce a uniform rise in gas volume fraction across the column. A comparison of results from the two spargers indicates a significant change in development length with the number and size of sparger holes.

NOMENCLATURE

D = diameter of bubble column, m
Mo = Morton number, dimensionless
P_{col} = column headspace pressure, kPa
R = radius of bubble column, m
Re = Reynolds number, dimensionless
U_G = superficial gas velocity, cm s^{-1}
We = Weber number, dimensionless
g = gravitational constant, 9.807 m s^{-2}
r = radial coordinate, m
x, y = Cartesian coordinates in measurement plane, m
z = axial coordinate, m
$\bar{\varepsilon}$ = volume-averaged phase volume fraction, dimensionless
$\langle\varepsilon\rangle$ = cross-sectionally-averaged phase volume fraction, dimensionless
ε = local phase volume fraction, dimensionless
η = dynamic viscosity, Pa·s
μ = gamma attenuation coefficient, cm^{-1}
ρ = density, g cm^{-3}
σ = surface tension, N m^{-1}

Subscripts
G gas phase
L liquid phase

INTRODUCTION

Slurry bubble-column reactors, or SBCRs, are vertical, large-diameter cylindrical pressure vessels in which a reactive gas is bubbled through a catalyst-laden liquid to produce a desired chemical. To assist in the design and scaleup of SBCRs, Sandia National Laboratories is conducting research on the hydrodynamic behavior of vertical multiphase flows. Current projects in this field are concerned with determining the effects of phase properties, sparger design, gas flow rates, and column pressure upon phase distributions in vertical bubble columns. The distribution of the phases is important because significant spatial variations can induce large-scale, buoyancy-driven motions that can reduce gas residence time in a reactor and thus decrease process efficiency. The flow regime in which a reactor operates also affects these quantities, so it is important to determine the values of operating parameters at which flow regime transitions – such as transitions from homogeneous bubbly flow to churn-turbulent flow – occur.

Related research at Sandia involves the development and application of nonintrusive diagnostic methods on both laboratory and industrial scales. The eventual goal of this work is to use these diagnostics to determine the flow regime and phase distributions in SBCR vessels at conditions similar to those in industry. Such information can be used to improve indirect coal liquefaction and other industrial processes.

[1] Sandia is a multiprogram laboratory operated by Sandia Corporation, a Lockheed Martin Company, for the United States Department of Energy under Contract DE-AC04-94AL85000.

DISCLAIMER

An assessment of how sparger design affects the gas volume fraction distribution in an SBCR vessel is currently being performed in collaboration with Air Products and Chemicals and Washington University in Saint Louis, Missouri. Of particular interest is how the number, size, distribution, and direction of the holes through which the gas is injected into the liquid affect the development of the gas distribution. In the study described here, gamma-densitometry tomography is applied to measure the gas distributions in gas-liquid flows generated by different sparger designs. Results are presented that will be used as detailed data sets for multiphase model development. Comparisons are also made to findings in other bubble-column hydrodynamics studies in the literature.

EXPERIMENTAL APPARATUS

Sandia SBCR Facility

The sparger studies are being conducted in a slurry bubble-column testbed installed at Sandia for hydrodynamic studies at industrially relevant conditions. The SBCR testbed, shown in Figure 1, has an inner diameter of 0.483 m and an inner height of 3.15 m. The column is rated for headspace pressures P_{col} up to 689 kPa gauge and temperatures up to 200° C. (Unless otherwise stated, all pressures in this paper are absolute.)

Typically, water or mineral oil is used as the liquid phase in these experiments. Drakeol™, a light mineral oil, is used to simulate the liquid used in the coal liquefaction process, but no chemical reaction takes place in the Sandia SBCR. Dry air is introduced into the column from a high-pressure air supply through one of several interchangeable spargers mounted at the bottom of the column. Air volumetric flow rates up to 3300 L min^{-1}, corresponding to superficial gas velocities U_G up to 30 cm s^{-1}, routinely produce churn-turbulent flow conditions in the column.

A total of 24 ports are placed along the column walls for viewing the flow or for use as instrumentation ports. The ports are at each of six levels that are spaced 0.457 m along the column height. Currently the column is extensively instrumented with pressure diagnostics at all levels and thermocouples at the column wall.

Sandia GDT System

The gamma-densitometry tomography (GDT) system developed at Sandia for studies of industrial-scale multiphase flows is shown in Figure 1 (Torczynski *et al.*, 1996; Shollenberger *et al.*, 1997). The system consists of a 5-curie ^{137}Cs gamma source, a sodium-iodide detector system, horizontal and vertical traverses that position the source and detector on opposite sides of the test object, and hardware and software for data acquisition and system control.

Gamma ray attenuation is measured along parallel beam paths through the column and translated into a gamma attenuation coefficient μ averaged along each path. The Abel transform (Vest, 1985) is then used to convert the path-averaged attenuation coefficients to a normalized radial attenuation profile in the circular domain. Finally, the radial attenuation profile is used to reconstruct a gas volume fraction distribution $\varepsilon_G(r)$ through the formula

$$\varepsilon_G(r) = \frac{\mu_L - \mu(r)}{\mu_L - \mu_G}, \qquad (1)$$

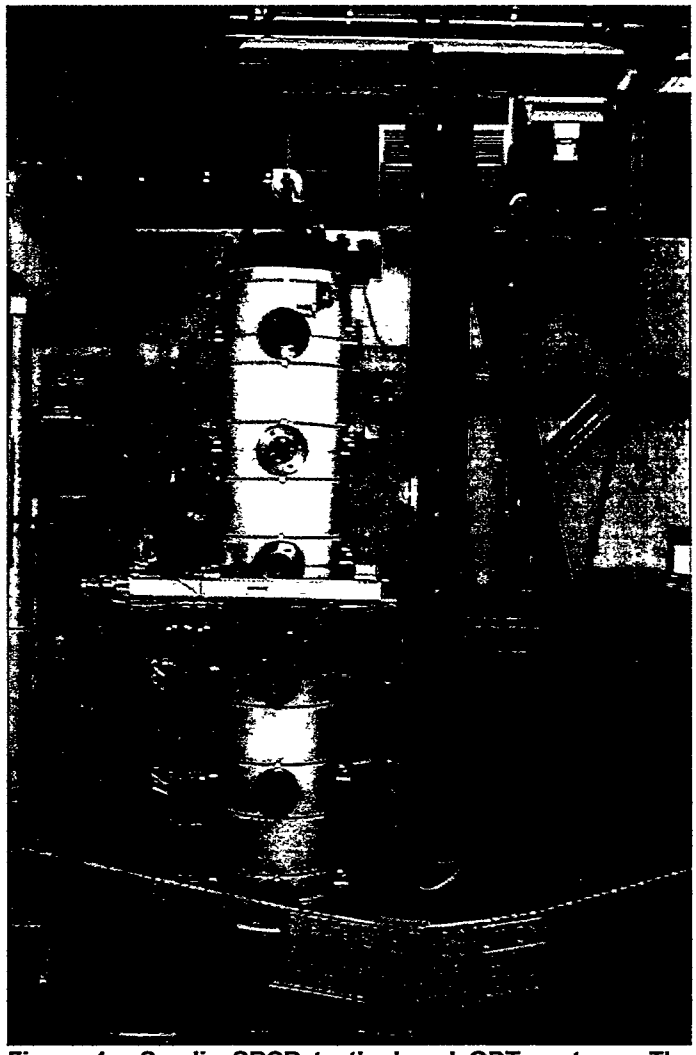

Figure 1. Sandia SBCR testbed and GDT system. The vertical traverse is to the right of the column; the gamma source and its horizontal traverse are visible in front.

where the gas and liquid attenuation coefficients are known *a priori*. The Abel transform uses the assumption of an axisymmetric phase distribution, an assumption that is valid for many vertical gas-liquid flows when averaged over long time scales. In the flows considered here, GDT measurements along one chord through the column are taken over the course of a full minute, and scans across a single plane require approximately 15 minutes. Hence, while gas volume fractions can be found from GDT data as a function of radial position or as volumetric averages, all measurements are inherently averages in time.

For the SBCR experiments, a 3-m vertical traverse has been constructed to allow GDT scans at several locations ranging from the vicinity of the sparger to the top of the liquid column. The vertical traverse transports the horizontal stage, which moves the source and detector in tandem on opposite sides of the column. This vertical traverse allows the effect of sparger parameters on radial and axial gas distribution in the bubble column to be determined in detail and also allows the flow development length to be determined for each sparger.

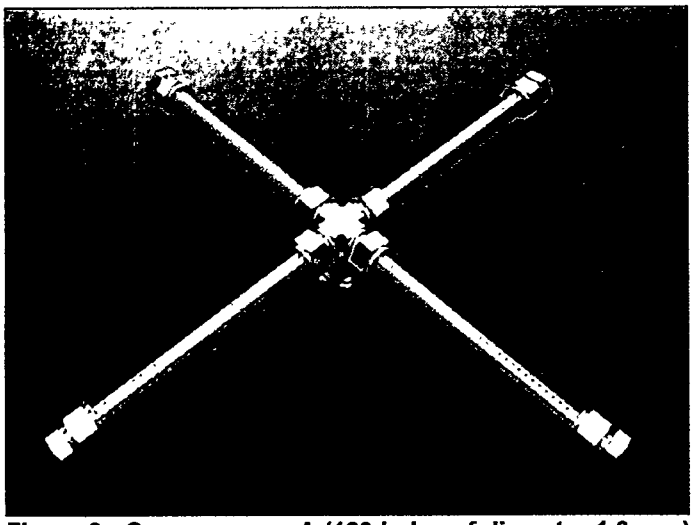

Figure 2. Cross sparger A (120 holes of diameter 1.0 mm) used in the SBCR hydrodynamics study.

Table 1. Specifications of the cross spargers built for this study.

Sparger geometry	Porosity	Number of holes	Hole dia. (mm)	Hole direction
A	0.0005	120	1.0	Up
B	0.0010	96	1.55	Up
C	0.0010	24	3.175	Up
D	0.0010	4	7.60	Up
E	0.0010	96	1.55	Down

Sparger Designs

To determine the effects of sparger hole size, location, and number on gas distributions within the gas-liquid flow, four cross-shaped spargers have been designed and built for the SBCR. Figure 2 is a photograph of sparger A, used in the first set of tests. All spargers are made of stainless steel, have identical arms of 1.59-cm ID stainless tubing, and have an arm span of 45.4 cm. The spargers are mounted in the vessel such that holes on the top of the arms are located $z = 0.176$ m above the vessel bottom, at a nondimensionalized height z/D of 0.36.

Table 1 lists the hole geometry of all sparger configurations to be tested and their resulting porosity, defined as the ratio of the total hole area to the area of the column. Most of the spargers have the same porosity of 0.0010, a value chosen to avoid sonic flow by the gas as it leaves the sparger holes. One-quarter of the total number of holes on each sparger resides on each of the four arms, and the holes are spaced evenly over a distance of 15.2 cm. Sparger geometry E will be produced by rotating the arms of sparger B so that the holes face downward; this geometry will test the effects of hole direction on gas distribution. In this case the holes will be located at an elevation of $z = 0.157$ m, or $z/D = 0.33$, above the vessel bottom.

TEST MATRICES

A test plan is underway to assess the hydrodynamic characteristics of the spargers over pressures and flow rates appropriate to industrial applications. For each sparger configuration, the column is initially filled with liquid to a depth of $z = 1.93$ m ($z/D = 4.0$). A matrix of up to six airflow rates and four or five headspace pressures is then applied. At each set of conditions, horizontal planes at several vertical locations are scanned using GDT to determine the gas phase distributions, average gas volume fractions, and development lengths in the flow. The full set of GDT measurements currently consists of data collected at eight vertical locations, $z = 0.546$ m to 2.146 m ($z/D = 1.1$ to 4.4) in steps of 0.229 m. Measurements are made along 11 chords across each plane, and gamma counts are collected for 60 s at each chord.

The first matrix of 22 conditions has been completed for sparger A using Drakeol 10 as the liquid phase. This grade of Drakeol has a density of 846 kg m^{-3}, a viscosity of 0.031 Pa·s, and a surface tension with air of 0.032 N m^{-1}. In all, five values of P_{col} were employed: 103 kPa through 517 kPa in increments of 103 kPa. Six values of U_G were also applied: 5 cm s^{-1} through 30 cm s^{-1} in increments of 5 cm s^{-1}. Some conditions in the potential 5×6 test matrix could not be achieved for practical reasons, resulting in only 22 tests being performed. For example, because of the exhaust line geometry, a superficial gas velocity of 30 cm s^{-1} produces a minimum headspace pressure of 170 kPa, preventing data from being obtained at 30 cm s^{-1} and 103 kPa.

A reduced test matrix of 14 conditions over the same parameter space has also been completed using Drakeol 10 and sparger D. This matrix incorporated the same range of superficial gas velocities, but based on the small changes in gas volume fraction with column pressure observed during tests with sparger A, no tests were performed at 414 kPa.

RESULTS AND DISCUSSION

The process for reconstructing gas volume fraction profiles is illustrated in Figure 3. The data points in the graph are chord-averaged gas volume fractions obtained by applying Eq. 1 to GDT attenuation measurements along each beam path. Unlike the final radial phase profile, each chord-averaged value at $x = r$ incorporates phase information over a range of radial positions from r to R, as shown in the diagram. The dashed line in the graph indicates the fit to the chord-averaged gas volume fraction data; the fit was obtained by applying Eq. 1 directly to the fit of chord-averaged attenuation data. Finally, through the Abel transform and Eq. 1, the attenuation curve in x is converted to the radial gas volume fraction profile in r (the solid line). A fourth-order polynomial was chosen to fit the raw data in all reconstructions; in the typical case of Figure 3, the average absolute deviation between the raw data and the curve fit is 0.004 in ε_G.

From the GDT attenuation measurements, radial and axial distributions of gas volume fraction were determined for each flow condition. Some of the experiments at a given condition were duplicated to establish the repeatability of results. Local values of gas volume fraction varied, typically, by 0.01 or less between repeated cases. This may reflect the effects of differences in column pressure and superficial gas velocity between "identical" cases (3 to 17 kPa and 0.1 to 0.8 cm s^{-1}, respectively); however, these differences in ε_G between cases are also on the order of the estimated uncertainty in GDT measurements of ±0.01 (George *et al.*, 1999). The measurements are thus considered repeatable to within experimental uncertainty.

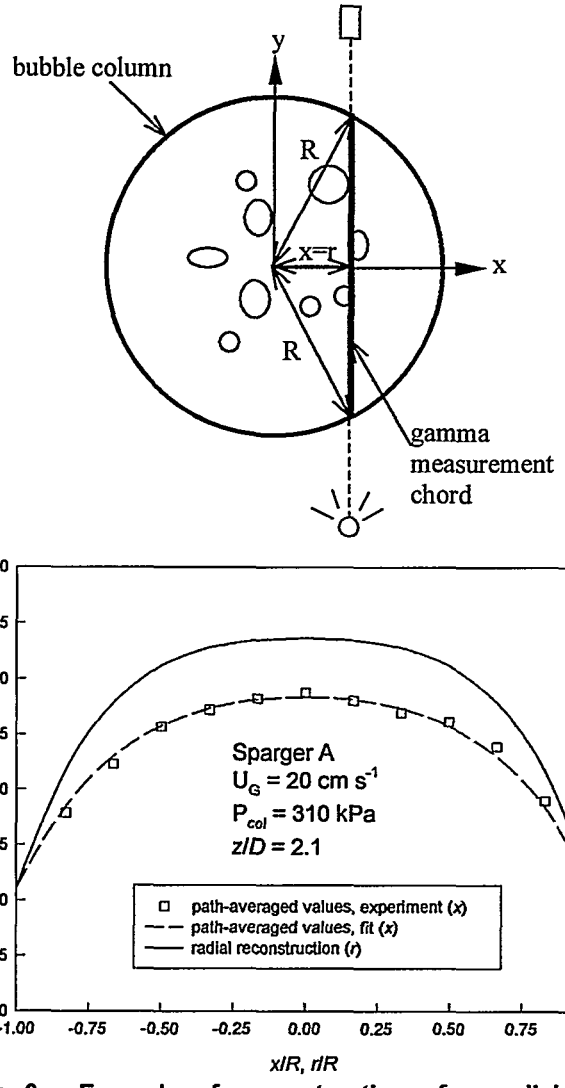

Figure 3. Example of reconstruction of a radial gas volume fraction distribution from chord-averaged data. Top: geometry of a measurement chord formed by a gamma path. Bottom: comparison of path-averaged values (in *x*) with the radial reconstruction (in *r*).

Sparger A results

Figure 4 shows the volume-averaged gas volume fraction $\bar{\varepsilon}_G$ in the column as a function of superficial gas velocity U_G and headspace pressure P_{col}, for all the conditions tested in the sparger A matrix. Integration of the gas volume fraction profiles over each scan plane is used to obtain cross-sectional averages $\langle \varepsilon_G \rangle$. Since the GDT scan planes are evenly spaced, a simple average is then taken over the vessel volume of values of $\langle \varepsilon_G \rangle$ in the developed flow region from $z/D = 1.6$ to 3.5 to determine the volume averages, $\bar{\varepsilon}_G$.

Correlations for average gas volume fraction commonly cited in the literature (Akita and Yoshida, 1973; Wilkinson *et al.*, 1992; Deckwer and Schumpe, 1993; Joshi *et al.*, 1998) were obtained using significantly different sparger configurations and liquid column

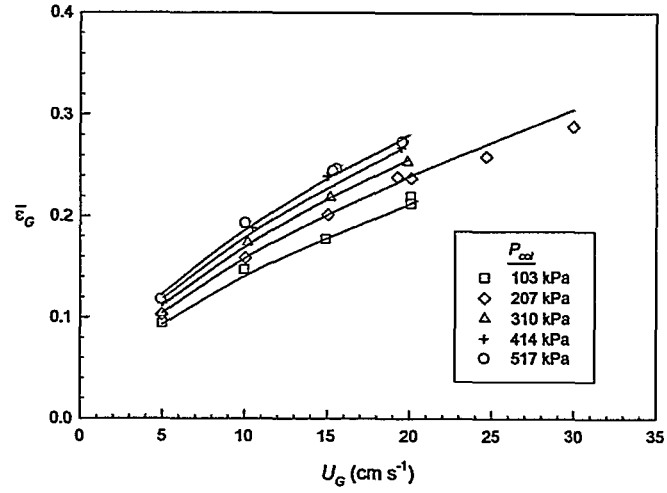

Figure 4. Column-average gas volume fraction as a function of superficial gas velocity and headspace pressure for sparger A.

dimensions than are found here and do not predict the measured values well. The following correlation was derived from the data in this work:

$$\bar{\varepsilon}_G = 2.0667\,\mathrm{Mo}^{0.0238}\left(\frac{\rho_G}{\rho_L}\right)^{0.1766}\left(\frac{\mathrm{We}_L}{\mathrm{Re}_L}\right)^{0.5949} \qquad (2)$$

The Morton number, a measure of the relative importance of viscosity to that of surface tension, is defined as

$$\mathrm{Mo} = \frac{g\eta_L^4}{\sigma^3 \rho_L}, \qquad (3)$$

and the Weber and Reynolds numbers are based on the liquid properties and the superficial gas velocity.

$$\mathrm{Re}_L = \frac{\rho_L U_G D}{\eta_L} \qquad (4)$$

$$\mathrm{We}_L = \frac{\rho_L U_G^2 D}{\sigma_L} \qquad (5)$$

This correlation is plotted as the solid lines in Figure 4; as seen in the figure, the correlation reproduces the measured gas volume fractions well except for the values at the two highest flow rates.

Variations in the cross-sectional average $\langle \varepsilon_G \rangle$ along the column height have been studied for all test conditions to investigate the effects of pressure and gas flow rate on development length. As an example, Figure 5 shows the variation of $\langle \varepsilon_G \rangle$ as a function of dimensionless height z/D above the bottom of the column, for all values of superficial gas velocity and a nominal headspace pressure of 207 kPa. Figure 6 similarly presents variations in $\langle \varepsilon_G \rangle$ with z/D and headspace pressure for a nominal superficial gas velocity of

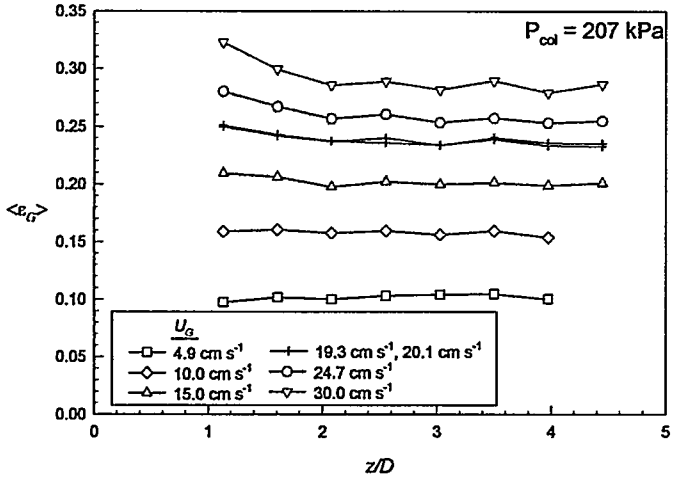

Figure 5. Average gas volume fraction versus dimensionless distance *z/D* above the column floor as a function of superficial gas velocity for sparger A.

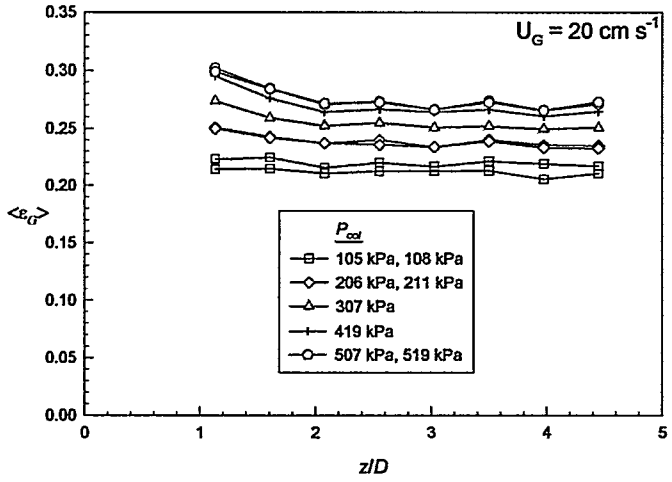

Figure 6. Average gas volume fraction versus dimensionless distance *z/D* above the column floor as a function of column pressure for sparger A.

U_G = 20 cm s^{-1}. The cross-sectional averages of gas volume fraction do not vary significantly with height for most test conditions. However, at the highest values of U_G and P_{col}, an entrance region or development region is evident. An appreciable decrease in gas volume fraction of 0.02 to 0.04 is seen with increasing height above the sparger at these conditions, a significant change compared to the uncertainty of about ±0.01 in ε_G. This entrance region is seen to occupy the first one or two diameters above the vessel bottom, and above *z/D* = 2, no significant variation is observed. It is also noted that the length of the entrance region appears to increase with U_G for a given headspace pressure and with P_{col} for a constant superficial gas velocity.

Changes in the gas volume fraction radial distribution $\varepsilon_G(r)$ with vertical position, headspace pressure, and flow rate have also been investigated. Figure 7 shows representative radial gas volume fraction profiles at all measurement locations for a nominal headspace

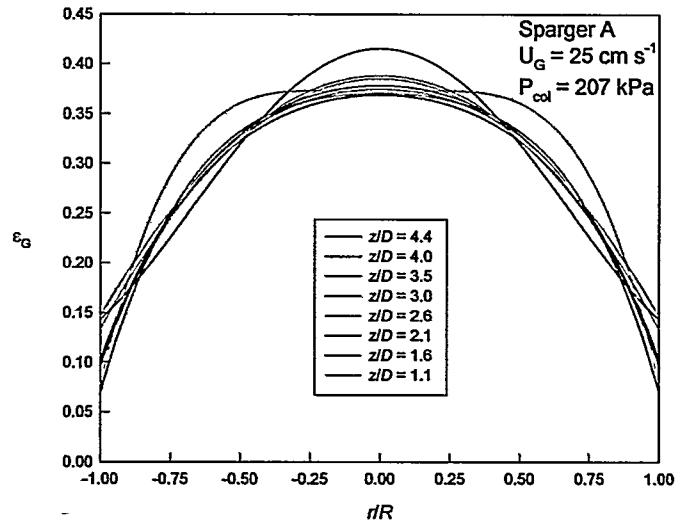

Figure 7. Typical gas volume fraction radial profiles as a function of axial height in the SBCR.

pressure of 207 kPa and a superficial gas velocity of 25 cm s^{-1}. The profiles are nearly identical at all elevations except for *z/D* = 1.1 (near the sparger, where the profile is noticeably flat toward the centerline) and *z/D* = 4.4 (near the free surface, where the profile is sharply peaked). For all flow conditions, fourth-order fits are consistently required at the lowest measurement level near the sparger to reconstruct the radial gradients in the gas volume fraction profile. At all higher locations a parabola adequately represents the profiles – *i.e.*, the fourth-order coefficient is small. This trend is identical to that demonstrated by multiple-hole spargers at ambient pressures and is the result of liquid circulation carrying bubbles toward the column center until the flow is fully developed (Joshi *et al.*, 1998). Except for the lowest and highest measurement locations, only a small variation in gas distribution with vertical location is observed. This is consistent with the development length observations made earlier from the values of $\langle \varepsilon_G \rangle$.

Figure 8 shows the variations in gas volume fraction radial profiles with superficial gas velocity and dimensionless vertical height for a nominal column pressure P_{col} of 207 kPa. For a fixed pressure and a particular height, an increase in U_G is seen to increase the local gas volume fraction more at the column axis than at the wall. This trend is in agreement with many other observations, most made at ambient pressures (Adkins *et al.*, 1996; Kumar *et al.*, 1997; Joshi *et al.*, 1998).

Similarly, Figure 9 shows $\varepsilon_G(r)$ as a function of *z/D* and P_{col} for a nominal superficial gas velocity U_G of 20 cm s^{-1}. Comparing profiles at a given axial height, an increase in headspace pressure at fixed U_G is seen to increase the gas volume fraction almost uniformly at all radial locations. These observations are in agreement with previously reported results for air-water and air-Drakeol 10 phase distributions (Adkins *et al.*, 1996; Torczynski *et al.*, 1997). Also, by comparing Figures 8 and 9, it can be seen that gas volume fraction profiles are more sensitive to changes in superficial gas velocity than changes in column pressure.

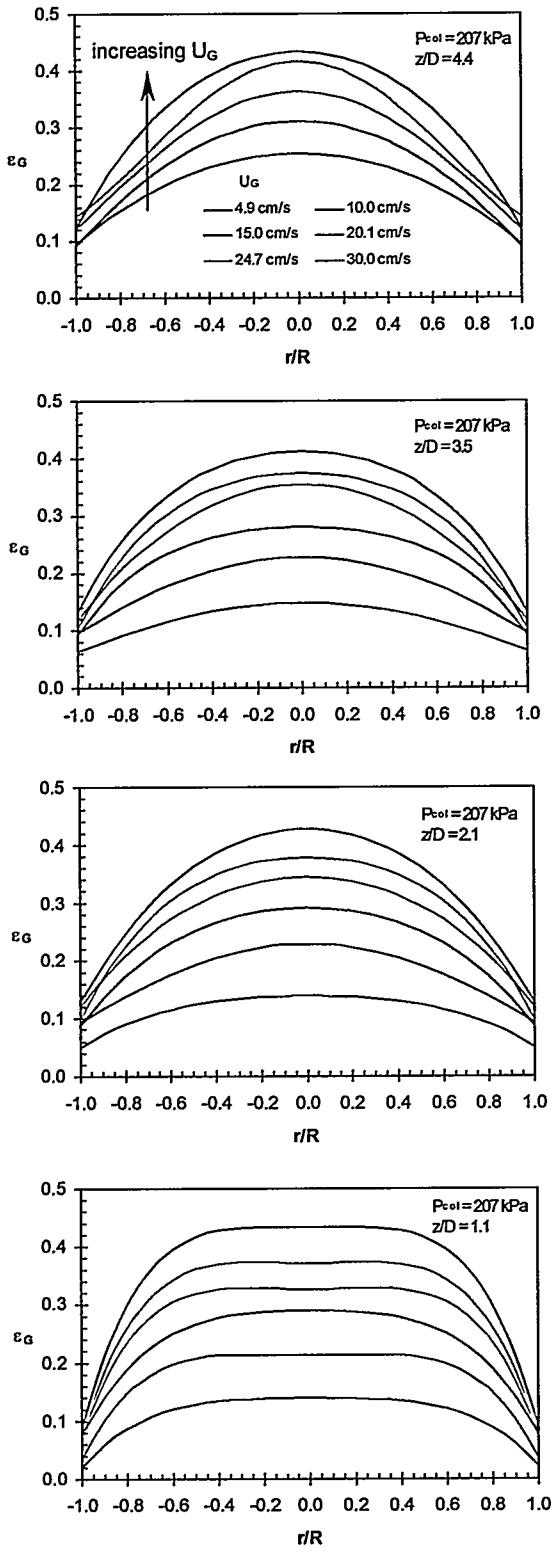

Figure 8. Gas volume fraction profiles as a function of superficial gas velocity and distance from the column bottom at a headspace pressure of 207 kPa. Sparger A was used to produce these flows. The legend for all cases appears in the top figure.

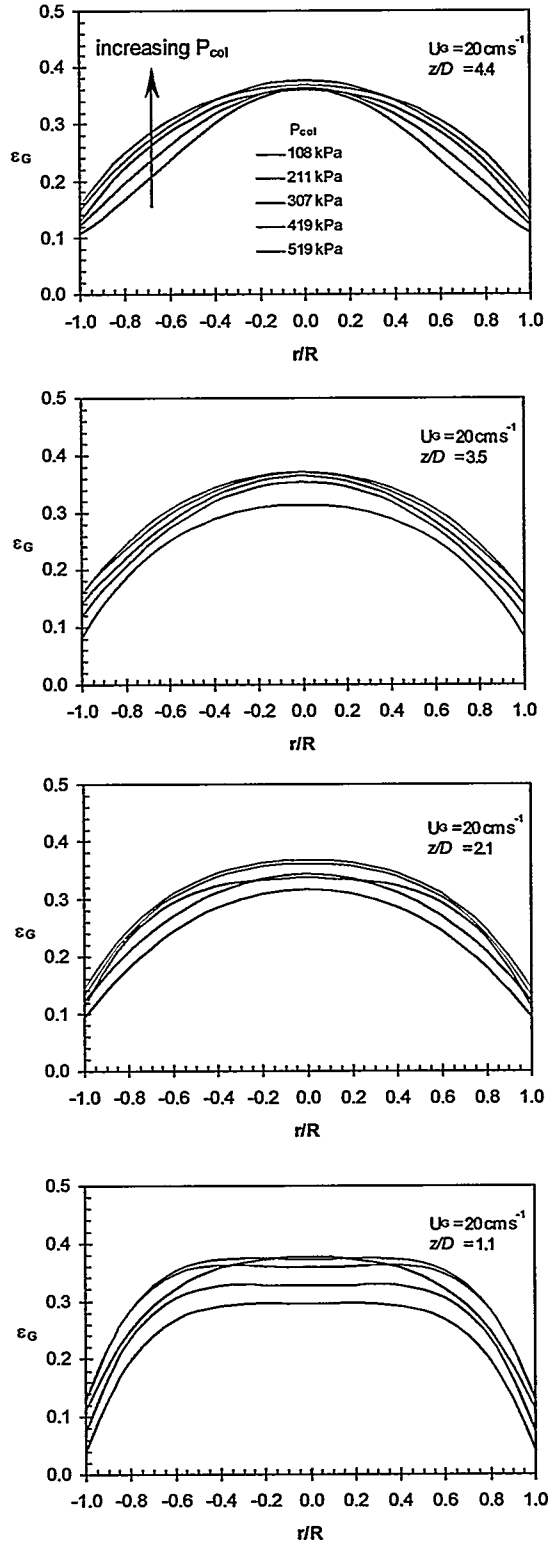

Figure 9. Gas volume fraction profiles as a function of headspace pressure and distance from the column bottom at a superficial gas velocity of 20 cm s^{-1}. Sparger A was used to produce these flows. The legend for all cases appears in the top figure.

Sparger D results

A reduced test matrix has been completed for sparger D, which differs the most in hole number and hole size from sparger A. Figure 10 shows the average gas volume fraction $\bar{\varepsilon}_G$ in the column as a function of U_G and P_{col} for all conditions tested in the sparger D matrix. As before, an average is taken using the cross-sectional profiles from $z/D = 1.6$ to 3.5 to determine $\bar{\varepsilon}_G$. Predictions from the correlation developed from sparger A data (Eq. 2) are also graphed as solid lines in Figure 10. It is evident that the sparger A correlation also predicts results from sparger D well, suggesting that differences in hole size and number have little influence on the column average gas volume fraction.

Figure 11 shows the cross-sectional average values $\langle \varepsilon_G \rangle$ as a function of dimensionless height z/D above the bottom of the column, for a nominal pressure of 207 kPa and six different flow rates from sparger D. Results from sparger A at the same pressure and nominal flow rates (Figure 5) are repeated in Figure 11 with dashed lines. The flows generated by spargers A and D have similar average gas volume fractions except at the lowest level near the sparger. Notably, at 20 cm s^{-1} and below, $\langle \varepsilon_G \rangle$ increases with height to the equilibrium value at $z/D = 1.6$ in the case of sparger D but remains steady with height or decreases to the same equilibrium value in the sparger A tests. Explanations for this behavior are being investigated.

While the cross-sectional average values from the two spargers exhibit the same trends and similar values beyond $z/D = 1.6$, the radial profiles are clearly very different, as seen by comparison of Figure 7 and Figure 12. The profiles from sparger D shown in Figure 12 progress from a quartic profile with severe gradients at $z/D = 1.1$ to a familiar parabolic curve at $z/D = 4.4$, and the gas volume fraction on the column centerline continually increases with axial height. The profiles from sparger D were produced using quartic curve fits at all axial locations. Even at the level nearest the sparger, quartic fits are plausible representations of the data, as demonstrated in Figure 13. Fits of higher order produced less deviation from the data but yielded physically unreasonable gas volume fraction profiles.

The progression of these profiles with height indicates that a fully developed, parabolic gas volume fraction profile is not obtained from sparger D until about $z/D = 3.5$, much further up the column than with sparger A. It is concluded from the profile data that the change in development lengths between flows from the two spargers is significant, and that radial profiles are more useful than cross-sectional averages in characterizing the development length of the gas-liquid flow.

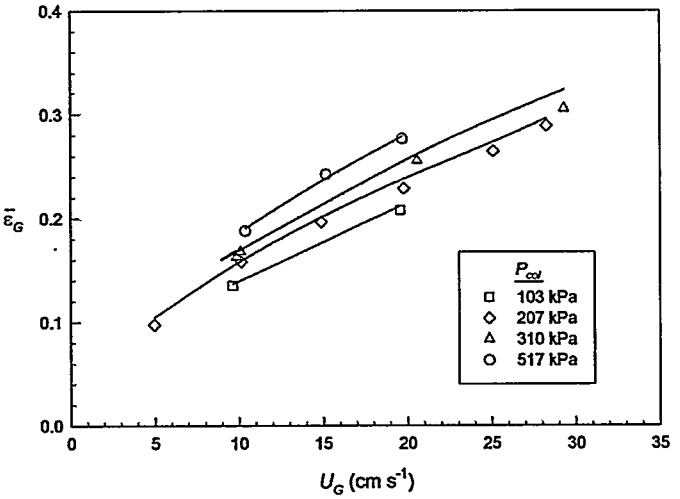

Figure 10. Column-average gas volume fraction as a function of superficial gas velocity and headspace pressure for sparger D.

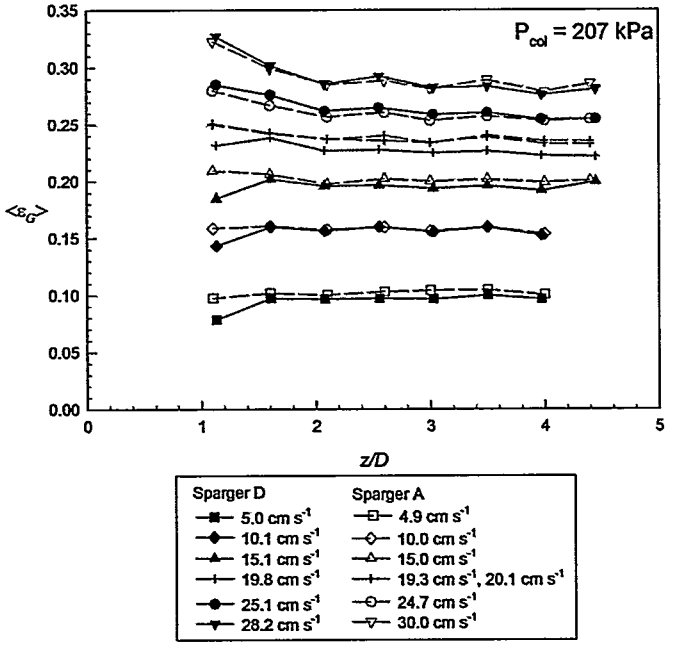

Figure 11. Average gas volume fraction versus dimensionless height as a function of superficial gas velocity and column pressure for both spargers tested to date.

CONCLUSIONS

Gamma-densitometry tomography has been applied to measure the effects of gas flow rate and pressure on gas phase distributions for two sparger geometries in a bubble-column testbed. Increases in the gas flow rate are seen to increase the local gas volume fraction preferentially on the column axis, in agreement with investigations of vertical gas-liquid flows at ambient conditions. The effect of column headspace pressure on the gas distribution has been considered less often in the literature; increases in column pressure in this study resulted in an increase in gas volume fraction by a constant value across the entire column. The development length of the gas volume fraction profile was also investigated and found to increase with both gas flow rate and column pressure.

The effects of sparger hole geometries on gas distributions are of primary concern in this study. Gas-liquid flows have been generated with a sparger containing 120 holes at a porosity of 0.0005 and a sparger containing 4 holes at a porosity of 0.0010. Comparisons of gas-liquid flows created by both spargers reveal a significant difference in the vertical development length of the gas volume fraction radial distributions. The difference in the cross-sectionally-averaged gas volume fractions of the two flows is small, however.

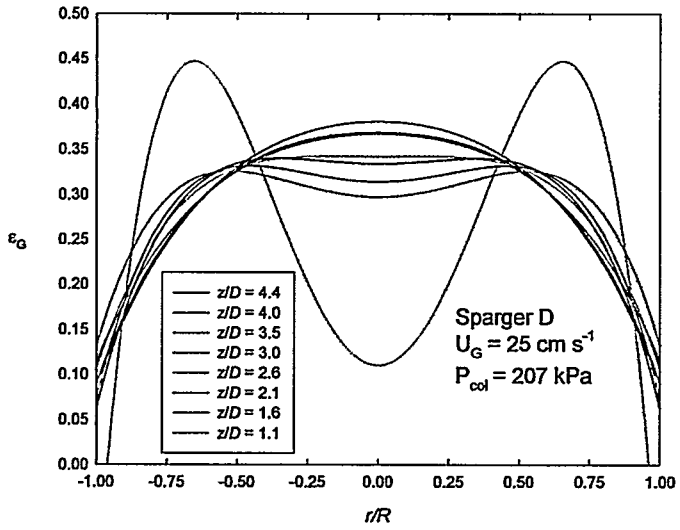

Figure 12. Gas volume fraction radial profiles as a function of axial height produced by sparger D.

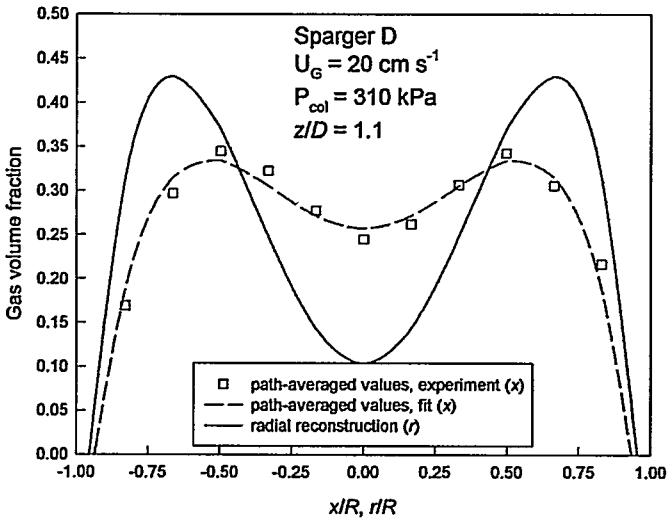

Figure 13. Reconstruction of radial gas volume fraction distribution at measurement plane nearest sparger D.

Further experiments will be conducted using spargers with porosities and numbers of holes between these two extreme cases. GDT scans will again be taken at the same eight vertical locations, and the results will be studied to determine the role of hole size and sparger porosity on gas phase distribution and flow development.

Experiments are also planned with Drakeol 5, an oil of significantly lower viscosity than Drakeol 10. These tests are intended to determine the effects of liquid viscosity on development length and radial gas distribution. The final matrix of gas distribution measurements as a function of flow rate, pressure, sparger design, and liquid viscosity will eventually be used as benchmark data for multiphase numerical code development.

REFERENCES

Adkins, D. R., Shollenberger, K. A., O'Hern, T. J., and Torczynski, J. R. , 1996, "Pressure Effects on Bubble-Column Flow Characteristics," *ANS Proceedings of the 1996 National Heat Transfer Conference*, American Nuclear Society, LaGrange Park, Illinois, THD-Vol. 9, pp. 318-325.

Akita, K., and Yoshida, F., 1973, "Gas Holdup and Volumetric Mass Transfer Coefficient in Bubble Columns," *Industrial and Engineering Chemistry Process Design and Development*, Vol. 12, pp. 76-80.

Deckwer, W.-D., and Schumpe, A., 1993, "Improved Tools For Bubble Column Reactor Design and Scale-Up," *Chemical Engineering Science*, Vol. 48, pp. 889-911.

George, D. L., Torczynski, J. R., Shollenberger, K. A., O'Hern, T. J., and Ceccio, S. L., 1999, *Quantitative Tomographic Measurements of Opaque Multiphase Flows*, Sandia National Laboratories, Albuquerque, NM, in press.

Joshi, J. B., Veera, U. P., Prasad, C. V., Phanikumar, D. V., Deshphande, N. S., Thakre, S. S., and Thorat, B. N., 1998, "Gas Hold-Up Structure in Bubble Column Reactors," *Proceedings of the Indian National Science Academy*, Part A, Vol. 64, pp. 441-567.

Kumar, S. B., Moslemian, D., and Dudukovic, M. P., 1997, "Gas-Holdup Measurements in Bubble Columns Using Computed Tomography," *AIChE Journal*, Vol. 43, pp. 1414-1425.

Shollenberger, K. A., Torczynski, J. R., Adkins, D. R., O'Hern, T. J., and Jackson, N. B., 1997, "Gamma-Densitometry Tomography of Gas Holdup Spatial Distribution in Industrial-Scale Bubble Columns," *Chemical Engineering Science*, Vol. 52, pp. 2037-2048.

Torczynski, J. R., Adkins, D. R., Shollenberger, K. A., and O'Hern, T. J., 1996, "Application of Gamma-Densitometry Tomography to Determine Phase Spatial Variation in Two-Phase and Three-Phase Bubbly Flows," *ASME Cavitation and Multiphase Flow Forum,* J. Katz and K. J. Farrell, eds., American Society of Mechanical Engineers, New York, FED-Vol. 236, pp. 503-508.

Torczynski, J. R., O'Hern, T. J., Adkins, D. R., Jackson, N. B., and Shollenberger, K. A., 1997, *Advanced Tomographic Flow Diagnostics for Opaque Multiphase Fluids*, Report SAND97-1176, Sandia National Laboratories, Albuquerque, NM.

Vest, C. M., 1985, "Tomography for Properties of Materials that Bend Rays: a Tutorial," *Applied Optics,* Vol. 24, pp. 4089-4094.

Wilkinson, P. M., Spek, A. P., and van Dierendonck, L. L., 1992, "Design Parameters Estimation for Scale-Up of High-Pressure Bubble Columns," *AIChE Journal*, Vol. 38, pp. 544-554.